Title: Role of the sintering atmosphere in the densification and phase composition of asymmetric BCZY-GDC composite membrane

Authors: Daniel Montaleone, Elisa Mercadelli, Angela Gondolini, Matteo Ardit, Paola Pinasco, Alessandra Sanson

PII: S0955-2219(18)30071-2
DOI: https://doi.org/10.1016/j.jeurceramsoc.2018.01.043
Reference: JECS 11711

To appear in: *Journal of the European Ceramic Society*

Received date: 9-8-2017
Revised date: 8-1-2018
Accepted date: 28-1-2018

Please cite this article as: Montaleone D, Mercadelli E, Gondolini A, Ardit M, Pinasco P, Sanson A, Role of the sintering atmosphere in the densification and phase composition of asymmetric BCZY-GDC composite membrane, *Journal of The European Ceramic Society* (2010), https://doi.org/10.1016/j.jeurceramsoc.2018.01.043

Role of the sintering atmosphere in the densification and phase composition of asymmetric BCZY-GDC composite membrane

Daniel Montaleone[1], Elisa Mercadelli*[1], Angela Gondolini[1], Matteo Ardit[2], Paola Pinasco[1], Alessandra Sanson[1]

[1]Institute of Science and Technology for Ceramics, National Council of Research (ISTEC-CNR), Via Granarolo 64, 48018, Faenza, Italy

[2]Department of Physics and Earth Sciences, University of Ferrara, Via Saragat 1, 44122 Ferrara, Italy

* Corresponding author: elisa.mercadelli@istec.cnr.it, Tel.: +39 0546699743, fax: +390546 46381

Abstract

Ceramic hydrogen separation membranes are promising devices to be integrated in industrial hydrogen-based technologies using fossil fuel as feedstock. Among all, $BaCe_{0.65}Zr_{0.20}Y_{0.15}O_{3-\delta}$ – $Ce_{0.8}Gd_{0.20}O_{2-\delta}$ composite membrane is the most promising ceramic-ceramic system for such application. However, one of the main issues in Ba-containing perovskites is related to Ba loss at the high sintering temperature needed for the complete densification of the material. This work reports the influence of the sintering atmosphere and temperature on the membrane's densification and phase purity. $BaCeO_3$ (BC), $BaCe_{0.65}Zr_{0.20}Y_{0.15}O_{3-\delta}$ (BCZY) and a $BaCe_{0.65}Zr_{0.20}Y_{0.15}O_{3-\delta}$ – $Ce_{0.8}Gd_{0.20}O_{2-\delta}$ (BCZY-GDC) mixture were used as Ba-sources to modify the sintering atmosphere. The more reactive BC and BCZY systems promoted a solid-state reaction between BCZY and GDC leading to an undesired single mix-phase enriched in barium on the membrane's surface. The desired asymmetric architecture with the correct stoichiometry was obtained using BCZY-GDC as Ba-source and sintering the membrane at 1550°C.

KEYWORDS: BCZY-GDC, TAPE CASTING, ASYMMETRIC MEMBRANE, HYDROGEN SEPARATION

1. Introduction

The worldwide increasing environmental concern is a strong incentive for using hydrogen (H_2) as a sustainable and clean energy source. To date, H_2 for industry has been mainly produced through the processing of the carbon-based

feedstock as schematized in Figure 1 [1]. As showed, the main product of the main processes is the syngas, therefore the separation step is mandatory to obtain pure H_2.

The associated H_2 separation processes that are based on pressure swing adsorption (PSA) or cryogenic distillation nonetheless are cost and energy intensive [2,3]. A low cost H_2 separation process is thus required to promote the large scale H_2 production and to realize the future hydrogen economy. Membrane separation technology can provide high H_2 permeation flux, small environmental footprint, and process intensification opportunity with low operational cost [2,4].

Among the available H_2-selective membrane candidates, the all-ceramic based ones are the most promising to obtain low-cost membranes with high chemical and thermal stability. In this context, doped perovskites, in particular the solid solutions of barium cerate and barium zirconate, have been exploited in recent years as proton conducting electrolytes in intermediate-temperature solid-oxide fuel cell (IT-SOFC) [5,6] and hydrogen separation membranes [7,8]. Among the others, yttrium-doped barium cerate zirconate solid solution represents a suitable compromise between good stability in CO_2 and H_2O containing atmosphere and high proton conductivity [9,10]. However, the low electron conductivity of these systems in reducing atmosphere strongly limits their applicability in pressure-driven hydrogen separating membrane technology. To overcome this issue, efforts have been made to couple a proton conducting perovskite with a suitable ceramic electron conductor (such as CeO_2 or $Ce_{1-x}Gd_xO_{2-\delta}$) to produce a dense ceramic-ceramic (cer-cer) composite [11,12]. In this way, the membrane can separate hydrogen without the aid of an external circuit. The proton and electron species formed by the hydrogen dissociation can, in fact, migrate through the membrane driven by the gradient of hydrogen partial pressure. Among the other cer-cer systems whose compositions and performances have been recently summarized by Wang et al. [13], Rebollo et al. reported exceptional performances for a ≈650 μm-thick $BaCe_{0.65}Zr_{0.20}Y_{0.15}O_{3-\delta}$ – $Ce_{0.85}Gd_{0.15}O_{2-\delta}$ (BCZY-GDC, 50-50 vol.) all-dense membrane, reaching hydrogen fluxes as high as 0.27 mL min^{-1} cm^{-2} at 755°C [14]. Since the hydrogen permeation is generally inversely proportional to the thickness of the membrane, performances may be enhanced with an asymmetric membrane architecture comprised of a thin membrane layer supported by a thick porous substrate. Hamakawaet al. [15] evaluated the effectiveness of this approach measuring the hydrogen flux for a 2 μm dense $SrCe_{0.95}Yb_{0.05}O_{3-\delta}$ membrane supported on a porous layer having the same composition. Such asymmetric membrane showed hydrogen fluxes 500 times higher than the one achieved by a 1 mm thick dense membrane of the same material. It is therefore possible to assume a strong increase in the hydrogen flux of the BCZY-GDC membrane in an asymmetric architecture.

Previous studies [16], however, highlighted some issues linked to the densification of the supported active thin membrane when in asymmetric configuration. The work showed that BaO loss from the BCZY lattice occurred during the sintering step with a detrimental effect on the densification of the 20 μm thick $BaCe_{0.65}Zr_{0.20}Y_{0.15}O_{3-\delta}$ –

$Ce_{0.80}Gd_{0.20}O_{2-\delta}$ membrane layer. This phenomenon is attributed to the favorable formation energy of Ba and O vacancy pairs [17] that consequently modify the BCZY stoichiometry and properties [18,19]. Since BaO evaporation starts from the surface, only the superficial portion of the material is involved in compositional and microstructural changes. Therefore, a light mechanical abrasion of the surface is sufficient and commonly considered to obtain a 1-2 mm thick disc with the desired composition and stoichiometry [20]. This expedient, however, cannot be applied for asymmetric architectures, due to the low thickness of the dense membrane layer.

In the present work, cer-cer asymmetric membranes consisting of a dense 20 µm thick active BCZY-GDC layer and a porous 600 µm thick BCZY support were produced by tape casting and lamination. The sintering atmosphere during the thermal treatment of the tape cast membrane was modified using different Ba-sources. An accurate evaluation of the effect of different barium sources on the density and phase purity of the thin BCZY-GDC membrane layer was done assessing the importance of the right amount of Ba in the sintering atmosphere for the production of dense separation membranes with the correct stoichiometry in asymmetric configuration.

2. Experimental

The asymmetric BCZY-GDC/BCZY membranes were produced as described elsewhere [16]. For the production of the dense membrane, ZnO (Sigma Aldrich) was directly added to the BCZY-GDC tape casting suspension to promote the membrane densification. The total amount of the sintering aid was fixed at 0.7 wt %. Samples were then debinded and sintered at 1450°C or 1550°C for four hours.

Three different powder systems were used as sources of barium during sintering: $BaCeO_3$ (BC, d_{50} = 0.9 µm and SSA = 3.65 m^2/g, supplied by Praxair), $BaCe_{0.65}Zr_{0.20}Y_{0.15}O_{3-\delta}$ (BCZY, d_{50} = 0.25 µm and SSA = 12.2 m^2/g, supplied by Marion Technology) and a 50/50 vol% mixture of $BaCe_{0.65}Zr_{0.20}Y_{0.15}O_{3-\delta}$ and $Ce_{0.80}Gd_{0.20}O_{2-\delta}$ (BCZY-GDC; GDC with SSA = 6.8 m^2/g, supplied by Fuel Cell Materials).

To control the sintering atmosphere, the Ba-containing powders were placed onto green asymmetric membranes of 26 mm in diameter and encapsulated with a zirconia crucible to seal the atmosphere. In this way, the active BCZY-GDC layer was put directly in contact with the Ba-source.

Thermogravimetric (TG) analyses (STA 449, Netzsch, Selb/Bavaria, Germany) were performed to assess the thermal stability of the three powders used as Ba-sources in the range 25-1550°C in air flux and with a heating rate of 5°C/min, while their chemical composition before and after the thermal treatment at 1550°C for 4 hours was assessed by semi-quantitative analysis with an EDS probe (EDS, X-Act, INCA Energy 300, Oxford Instruments, Abingdon, UK). The

microstructure of the sintered membranes was investigated by scanning electron microscopy (SEM-FEG, Carl Zeiss Sigma NTS GmbH, Oberkochen, Germany), embedding the cross sections under vacuum in epoxy resin and then polishing them down to 0.25 μm finish. The microstructure of the samples was observed and Ba- and Gd-element profiles were recorded using the EDS probe. To check the composition of the cer-cer membrane layer, XRD analyses were performed on the dense surface at room temperature using a Bruker D8 Advance diffractometer (Bruker AXS GmbH, Karlsruhe, Germany) on a Bragg-Brentano geometry with an X-ray tube operating at 40 kV and 40 mA. Data were collected through a one-dimensional LynkEye detector based on silicon strip technology, set to discriminate Cu $K\alpha_{1,2}$ radiation, in the 10-80° 2θ measuring range, with an equivalent counting time of 10s per 0.02° 2θ step anode X-ray. Phase analysis of XRD collected data were performed by means of HighScore Plus v.3.0 (PANalytical B. V., Almelo, The Netherlands). EXPGUI v.1208 interface [21] for the GSAS [22] was used to achieved quantitative phases analysis and unit-cell parameters perovskite main phase from X-ray diffraction data of the dense layer surfaces of the samples sintered at 1450°C and 1550°C used as Ba-source. The chemical composition of the dense membrane surfaces was assessed by semi-quantitative analysis with EDS probe. The porosity of the BCZY-GDC membrane layers and of the BCZY support layers were determined by image analysis of the polished cross-sections using the software ImageJ.

3. Results and Discussion

3.1 Ba-sources characterization

To assess the thermal stability of the different Ba-sources, the as-received powders were characterised through thermogravimetric analysis. The thermal stability of the selected systems is, in fact, a crucial parameter that must be considered in order to modify and control the sintering atmosphere at high temperatures. The TG curves of the three powders are reported in Figure 2.

The mass loss in the 25-200°C range is due to the evaporation of the water adsorbed on the surface of the powders, while the 200-700°C range is related to the dehydration of the perovskite lattice, mainly due to the water incorporation promoted by the oxygen vacancies. As reported by Kruth et al. [22] in fact, the amount of water contained in ambient condition is enough to fully hydrate Ba containing perovskites. Since the water incorporation into oxygen vacancies is fully reversible, a weight loss then occurs heating up the sample as described by the Equation:

$$2OH_O \leftrightarrow H_2O \uparrow + V_{\ddot{O}} + O_O^x \quad (1)$$

In the 700-1550°C range two distinct events may occur: the $BaCO_3$ decomposition and the BaO evaporation (Equations (2) and (3)):

$$BaCO_3 \leftrightarrow BaO\uparrow + CO_2 \quad (2)$$

$$BaCeO_3 \leftrightarrow xBaO\uparrow + Ba_{(1-x)}CeO_{(3-\delta)} \quad (3)$$

The presence of the barium carbonate is due to the low chemical stability of the barium cerate materials that under atmospheric condition, undergo to easy carbonation:

$$BaCeO_3 + xCO_2 \leftrightarrow xBaCO_3 + Ba_{(1-x)}CeO_{(3-x)} \quad (4)$$

As described by Equation (4) the carbonation of the material leads to oxygen vacancies which cause added water uptake, in accordance with Equation (1).

According to equations (2) and (3), the mass loss in the range 700-1550°C is strictly related to the tendency of the Ba-source to release barium into the sintering atmosphere.

TG analyses show that the un-doped BC displays the lowest chemical stability, followed by BCZY and BCZY-GDC [9, 17]. The overall BC weight loss is 7.7 wt. %, of which 5.6 wt. % is due to H_2O evaporation/dehydration and 2.1% is due to decarbonation and Ba loss events.

The presence of $BaCO_3$ as associated phase in the BC system and its decomposition at elevated temperatures was also verified by the XRD analyses (Figure 3): the main peak attributed to the orthorhombic $BaCO_3$ phase at about 24° (2θ) disappeared after thermal treatment at 1550°C.

XRD analysis also revealed a slight shift of the diffraction pattern towards higher 2θ values after the TG analysis: this result is consistent with other works [9, 24], that report a contraction as a consequence of the barium loss from the BC lattice. It is worth to note that for the sacrificial systems, the $BaCO_3$ decomposition and the lattice contraction due to barium loss, are both sign of a enrichment in barium of the sintering atmosphere.

As expected, BCZY undergoes a lower weight loss: 2.7% in total and only 1.07 % related to decarbonation and BaO loss. The incorporation of Zr^{4+} in the perovskite lattice it is well-known to increase the perovskite structural stability

against carbonation and water uptake [24, 25]. As previously reported for the BC sample, XRD analysis in Figure 4 confirmed the presence of the barium carbonate also in the starting powder of BCZY.

Figure 4 further highlights that the peaks of the main perovskite phase after TGA undergoes a clear sharpening associated with an intensity increasing after the thermal treatment. The XRD spectrum of perovskite phase in the BCZY before the TG analysis presents broad peaks that seem to be splitted as indication of two perovskite phases with different chemistry. This can be explained by the carbonisation reaction of barium-based materials with the atmospheric CO_2, that according to Equation 4, leads to the coexistence of two perovskite phases containing different Ba amount, as already observed in literature [9, 11]. The powder after thermal treatment however (i.e. after TGA) is monophasic with an enhanced crystallinity.

Finally, the thermogravimetric curve of the BCZY-GDC mixture (Figure 2) showed lower weight loss than the single BCZY phase for the presence of GDC that reduces the total amount of BCZY. Even in this case, traces of $BaCO_3$ were detected by XRD analyses (Figure 5). Analogously to what reported for BCZY, the untreated BCZY-GDC system shows broad and splitted diffraction peaks for the BCZY phase that, after the thermal treatment, become monophasic. After TGA, peaks of BCZY and GDC are detectable, and no-secondary phases appear.

To evaluate the Ba evaporation from the different sources of barium during sintering, semi-quantitative EDS analyses were carried out on the powders of the three systems before and after being thermally treated at 1550°C for 4 hours (to mimic the sintering conditions). Table 1 reports the Ba/Ce atomic ratio values of the EDS results before and after the thermal treatment.

Semi-quantitative EDS analyses revealed that the Ba/Ce atomic ratio of the BC system decreased from 1.20 ± 0.02 to 1.04 ± 0.01 due to a 5 molar % of Ba loss at the high sintering temperature. As predicted by the TGA, the BCZY was a more stable Ba-source than BC, in fact the Ba loss assessed by EDS was only 1.5 molar %. In the case of BCZY-GDC, no Ba loss was detected. This may be due to the low amount of the BCZY phase in the overall system: the Ba loss results in this way below the detection limit of this technique.

Therefore, the analyses confirmed the general trend in terms of thermo-chemical instability: BCZY-GDC < BCZY < BC (from the most to the less stable Ba-source). As it will be discussed in the next paragraph, this different stability

differently affects the sintering atmosphere and therefore the microstructures and phase purity of the asymmetric membrane.

3.2 Effect of the Ba-sources on the asymmetric BCZY-GDC/BCZY microstructure

Figure 6 reports the SEM analysis performed onto the cross section of the membranes sintered with the three different Ba-sources at 1450°C and 1550°C for four hours.

The microstructural investigation shows that the modification of the sintering atmospheres highly affected the densification level. Only BC system led to a fully densified membrane layer at 1450°C. SEM micrographs at higher magnification of the fracture section (Figure 7) shows the presence of an intergranular glassy-phase, probably due to the formation of a liquid Ba-enriched phase, which promoted the grain mobility enhancing, as a consequence, the densification [26-27]. For sake of comparison, Figure 7 reports also the fresh fractures at higher magnification of the membranes sintered with BCZY: as shown, the glassy phase is seen only in the samples sintered with BC.

Increasing the sintering temperature to 1550°C, led to a substantial grain coarsening, and the fracture morphology switched from intergranular to transgranular, clear indication that the glassy-phase in the intergranular region weakened the grain boundaries.

On the other hand, the more thermally stable BCZY and BCZY-GDC systems led to a fully densified membrane layer only at 1550°C (Figure 6).

Table 2 summarizes the residual porosity calculated by the image analysis of the membrane layers sintered at the two temperatures under different atmospheres.

All the samples sintered at 1550°C showed a residual porosity < 1%, while at 1450°C the membrane sintered using BCZY displayed a residual porosity around 5% and the one with BCZY-GDC had a residual porosity of about 10%,

demonstrating that the BCZY-GDC system inadequately enriched the sintering atmosphere in barium at this temperature.

The influence of the different Ba-sources on the membrane grain size was evaluated analyzing the SEM micrographs of the dense membrane surfaces (Figure 8 and 9).

The BC system led to the lowest grain size at 1450°C for the presence of the glassy phase previously mentioned which promoted the grain mobility but hindered the grain growth. These results are consistent with those of Babilo et al., that reported that enriching in barium the sintering atmosphere of sintered yttrium-doped barium zirconate pellets led to fully densified materials with a slightly smaller grain size [28]. However, the average grain size increased from 0.3 ± 0.1μm to 1.8 ± 0.2μm at 1550°C due to the higher amount of barium released in the atmosphere. The more stable BCZY system led to a slightly higher grain size at 1450°C, with the average value of 0.4 ± 0.1μm, that increased up to 0.9 ± 0.1μm at 1550°C. Finally, he most stable BCZY-GDC system followed the same trend of BCZY, even if the registered average grain sizes were smaller at the two temperatures investigated (0.4 ± 0.1μm at 1450°C and 0.6 ± 0.1μm at 1550°C), probably as a consequence of a globally lower amount of Ba containing compound.

Also the influence of the sintering conditions on the porosity and shrinkage of the supporting layer was accurately investigated. Figure 10 a) and b) report the variation of porosity and shrinkage of the support under the different two sintering conditions.

It is evident that the sintering atmosphere not only affected the microstructure of the dense layer, but also influenced the porosity of the BCZY substrate and the shrinkage of the bilayer.

The membrane sintered with BC at 1450°C showed, in fact, the lowest shrinkage, maintaining a support porosity as high as 45%. However, the shrinkage strongly increased with the temperature, reaching at 1550°C the highest value among all the membranes studied. This behavior is due to the high quantity of barium released by BC. The formation of the glassy-phase at 1450°C promotes the grain mobility of the membrane layer without affecting the support porosity. Increasing the sintering temperature up to 1550°C, the high amount of barium released lead to the densification of the support with a consequent higher shrinkage of the bilayer. On the other hand, BCZY and BCZY-GDC systems slightly affected the support porosity even with the temperature increase, in accordance with their higher thermal stability.

Samples sintered with BC at 1450°C and with BCZY and BCZY-GDC at 1550°C showed a sufficiently dense membrane layer, with a porosity of the support higher than 40%.

2.3 Effect of the sintering atmosphere on the membrane phase composition

The evaporation of Ba could, in principle, affect the stoichiometry of the dense layer and therefore its properties. In order to check that, XRD and semi-quantitative EDS analyses were carried out on the dense surfaces of the membranes sintered in different Ba-enriched atmospheres. The EDS profiles of Ba and Gd elements were also recorded on the polished fractures to evaluate the distribution of BCZY and GDC along the membrane layers.

Figure 11 a) and b) show the backscattered SEM micrographs of the polished section and Ba/Gd-EDS profiles of the BC_1450 and BC_1550 membranes. The analyses revealed that although the BCZY and GDC phases are not discernible from the backscattered image, the Gd and Ba elements are evenly distributed along the whole thickness of the membrane. Thus, the sintering atmosphere modified with BC not only promoted the densification of the membrane layer even at low temperature, but it also produced an undesired single mix-phase as a consequence of a solid-state reaction between the two starting systems. Such reaction can be explained by the barium migration through the membrane layer and its dissolution into the BCZY and GDC lattices. This phenomenon led to an increase of the defect concentration which boosted the grain mobility and cation migration from one lattice to the other, promoting the formation of the new undesired phase. A similar solid-state reaction between $Ce_{0.8}Gd_{0.2}O_{1.9}$ and $BaCO_3$was exploited by Serra et al. to obtain a $BaCe_{0.8}Gd_{0.2}O_{3-\delta}$ protonic electrolyte [24]. As reported in Figure 11 c), the XRD patterns of the membranes sintered with BC_1450 and 1550 revealed the presence of a single perovskite orthorhombic phase (s.g., *Pmcn*) confirming the formation of a single phase.

Unlike with BC, samples sintered using BCZY retain at least some of the dual phase composition (Figure 12).

.

In the sample treated at 1550°C, the XRD analysis revealed the presence of the single perovskitic phase (s.g., *Pmcn*) in the superficial part, while the two phases were still detected in the inner part of the dense layer. This result confirms that the Ba coming from the BCZY promotes the solid-state reaction only in the very top of the dense surface, physically in contact with BCZY. In the 1450°C samples, on the other hand, (Figure 12 c)) there is clearly some GDC even if the phase content is only 3.4%.

Figure 13 shows that BCZY-GDC allowed the preservation of the dual phase composition throughout the whole membrane layer at both temperatures. The XRD analyses performed on the top of the dense layer confirmed in fact the presence both of the perovskite (BCZY) and fluorite-type (GDC) phases.

Phase composition and lattice parameters of the main perovskite phase of the dense layer surfaces of all samples are listed in Table 3.

The data obtained suggest that, since Ba^{2+} is the biggest cation among the elements constituting the BCZY-GDC material, the Ba dissolution into the lattice lead to cell expansion. The BC_1450 and 1550 membranes showed the highest cell volumes. The perovskite unit-cell volume for the sample sintered at 1550°C was equal to 335.8 $Å^3$, slightly higher than that obtained for the membrane sintered at 1450°C (335.3 $Å^3$). The single phase produced by the solid-state reaction of the BCZY_1550 membrane displayed a lower unit-cell volume (334.6 $Å^3$), showing that the dense layer of the new undesired phase detected by SEM analysis had a lower amount of Ba. This is due to higher stability of BCZY in respect to BC. Only BCZY-GDC samples showed unit-cell volume values comparable to the ones reported in literature [30,31]. In this case, a unit-cell volume increasing id detected from low to high sintering temperature, i.e., the perovskite unit-cell undergoes an expansion from 328.3 $Å^3$ to 329.7 $Å^3$, respectively, meaning that a higher sintering temperature promoted both Ba evaporation from the Ba-source and the Ba dissolution into the membrane lattice.
The different Ba content in the dense membrane surface was confirmed by semi-quantitative EDS spectra. Figure 14 reports the Ba/Zr atomic ratio values of the EDS results. A green BCZY-GDC pellet was also analyzed for comparison and the Ba/Zr value obtained (Ba/Zr = 4) was taken as reference.

The Ba amount in BC_1450 is more than double than the one of the reference, and it triplicates at 1550°C. Similarly, the dense membrane sintered with BCZY, showed a Ba/Zr value of 6 at 1450°C and a value closed to 8 at 1550°C. Only the less reactive BCZY-GDC allowed to achieve a Ba/Zr ratio value close to the reference one at both sintering temperatures.

4. Conclusions

To face Ba loss from the BCZY phase of the asymmetric membrane dense layer, the sintering atmosphere was modified introducing different Ba-sources during the thermal treatment. This study proves that the sintering atmosphere is a crucial parameter to obtain thin and dense membrane layer with the needed phase composition. The highest reactive Ba-source BC, other than promote the densification of the membrane layer, led to the formation of a single-phase material due to Ba dissolution into the BCZY and GDC lattices. Even the membrane sintered using BCZY as Ba source was completely densified at higher temperature (1550°C) but the formation of the undesired single phase occurred in the

first 3-4 μm of the dense membrane. The Ba dissolution into the perovskite and fluorite lattices due to the solid-state reaction was also confirmed by the unit-cell parameters of the phases considered. Only using the BCZY-GDC as Ba source, the desired phase composition was achieved and a membrane of suitable microstructure (20 μm-thick dense layer and 42 vol.% porous support) was obtained.

Acknowledgment

This work was funded by the agreement between the Italian Ministry of Economic Development and the Italian National Research Council "Ricerca di sistema elettrico", under the frame of the Project: “Materiali e tecnologie abilitanti per la ricerca di sistema elettrico: materiali e componentistica – Linea progettuale 1: Studio e sviluppo di membrane ceramiche a conduzione mista per la valorizzazione di gas da biomasse (separazione di H_2)”.

References

[1] R. D. Noble, S. A. Stern, Membrane Separations Technology – Principles and Aplications, Elsevier Science (1995) Amsterdam.

[2] S. Adhikari, S. Fernando, Hydrogen membrane separation techniques, Ind. Eng. Chem. Res 45 (2006) 875-881.

[3] S. D. Sharma, Gas cleaning: pressure swing adsorption, Elsevier (2009) 335-349.

[4] Y. Shang, L. Wei, X. Meng, B. Meng, N. Yang, J. Sunarso, S. Liu, CO2-enhanced hydrogen permeability of dual-layered A-site deficient $Ba_{0.95}Ce_{0.85}Tb_{0.05}Zr_{0.1}O_{3-\delta}$-based hollow fiber membrane, J. Membr. Sci. 546 (2018) 82–89.

[5] Z. Zhu, W. Sun, Z. Shi, W. Liu, Proton-conducting solid oxide fuel cells with yttrium-doped zirconate electrolyte films sintered at reduced temperatures, J. Alloys Compd. 658 (2016) 716-720.

[6] P. Sawant, S. Varma, B. N. Wani, S. R. Bharadwaj, Synthesis, stability and conductivity of $BaCe_{0.8-x}Zr_xY_{0.2}O_{3-\delta}$ as electrolyte for proton conducting SOFC, Int. J. Hydrogen Energy 37 (2012) 3848-3856.

[7] H. Matsumoto, T. Shimura, H. Iwahara, T. Higuchi, K. Yashiro, A. Kaimai, T. Kawada, J. Mizusaki, Hydrogen separation using proton-conducting perovskites, J. Alloy. Compd. 408-412 (2006) 456-462.

[8] D. Mendevev, A. Murashkina, E. Pikalova, A. Demin, A. Podias, P. Tsiakaras, $BaCeO_3$: Materials development, properties and application, Prog. Mater. Sci. 60 (2014) 72-129.

[9] E. Fabbri, A. D'Epifanio, E. Di Bartolomeo, S. Licoccia, E. Traversa, Tailoring the chemical stability of $Ba(Ce_{0.8-x}Zr_x)Y_{0.2}O_{3-\delta}$ protonic conductors for Intermediate Temperature Solid Oxide Fuel Cells (IT-SOFCs), Solid State Ionics 179 (2008) 558-564.

[10] K. Yang, J. X. Wang, Y. J. Xue, M. S. Wang, C. R. He, Q. Wang, H. Miao, W. G. Wang, Synthesis, sintering behaviour and electrical properties of $Ba(Zr_{0.1}Ce_{0.7}Y_{0.2})O_{3-\delta}$ and $Ba(Zr_{0.1}Ce_{0.7}Y_{0.1}Yb_{0.1})O_{3-\delta}$ proton conductors, Ceram. Int. 40 (2014) 15073-15081.

[11] D. Montaleone, E. Mercadelli, A. Gondolini, P. Pinasco, A. Sanson, On the compatibility of dual phase Ba $Ce_{0.65}Zr_{0.2}Y_{0.15}O_3$-based membrane for hydrogen separation application, Ceram. Int. 43 (2017) 10151-10157.

[12] S. Ricote, A. Manerbino, N.P. Sullivan, W. G. Coors, Preparation of dense mixed electron- and proton-conducting ceramic composite materials using solid-state reactive sintering: $BaCe_{0.8}Y_{0.1}M_{0.1}O_{3-\delta}$-$Ce_{0.8}Y_{0.1}M_{0.1}O_{2-\delta}$ (M=Y, Yb, Er, Eu), J. Mater. Sci. 49 (2014) 4332-4340.

[13] H. Wang, X. Wang, B. Meng, X. Tan, K.S. Loh, J. Sunarso, S. Liu,Perovskite-based mixed protonic–electronic conducting membranes for hydrogen separation: Recent status and advances, J. Ind. Eng. Chem. (2017), https://doi.org/10.1016/j.jiec.2017.11.016.

[14] E. Rebollo, C. Mortalò, S. Escolastico, S. Boldrini, S. Barison, J.M. Serra, M. Fabrizio, Exceptional hydrogen permeation of all-ceramic composite robust membranes based on $BaCe_{0.65}Zr_{0.20}Y_{0.15}O_{3-\delta}$ and Y- or Gd-doped ceria, Energy Environ. Sci. 8 (2015) 3675-3686.

[15] S. Hamakawa, L. Li, A. Li, E. Iglesia, Synthesis and hydrogen permeation properties of membranes based on dense $SrCe_{0.95}Yb_{0.05}O_{3-\alpha}$ thin films, Solid State Ionics 48 (2002) 71-81.

[16] E. Mercadelli, D. Montaleone, A. Gondolini, P. Pinasco, A. Sanson, Tape-cast asymmetric membranes for hydrogen separation, Ceram. Int. 43 (2017) 8010-8017.

[17] S. Barison, M. Battagliarin, T. Cavallin, L. Doubova, M. Fabrizio, C. Mortalò, S. Boldrini, L. Malavasi, R. Gerbasi, High conductivity and chemical stability of $BaCe_{1-x-y}Zr_xY_yO_{3-d}$ proton conductors prepared by a sol–gel method, J. Mater. Chem., 18 (2008) 5120-5128.

[18] D. Shima, S. M. Haile, The influence of cation no-stoichiometry on the properties of undoped and gadolinia-doped barium cerate, Solid State Ionics, 97 (1997) 443-455.

[19] S. Barison, M. Battagliarin, T. Cavallin, L. Doubova, M. Fabrizio, C. Mortalò, S. Boldrini, R. Gerbasi, Barium non-stoichiometry role on the properties of $Ba_{1+x}Ce_{0.65}Zr_{0.20}Y_{0.15}O_{3-\delta}$ proton conductors for IT-SOFCs, Fuel Cells 5 (2008) 360-368.

[20] C. Peng, J. Melnik, J. Luo, A. R. Sanger, K. T. Chuang, BaZr0.8Y0.2O3-δ electrolyte with and without ZnO sintering aid: preparation and characterization, Solid State Ionics, 181 (2010) 1372-1377.

[21] B. H. Toby, EXPGUI, a Graphical User Interface for GSAS. J. Appl. Crystallogr. 34 (2001) 210-213.

[22] A. C. Larson.; R. B. Von Dreele. General structure analysis system (GSAS); Los Alamos National Laboratory Report LAUR 86-748 (2004).

[23] A. Kruth, J. T. S. Irvine, Water incorporation studies on doped barium cerate perovskites, Solid State Ionics, 162 (2003) 83-91.

[24] C. Jin, Z. Huizhu, D. Lei, L. Yuehua, L. Wang, Effect of Ba nonstoichiometry on the phase composition, microstructure, chemical stability and electrical conductivity of $Ba_xCe_{0.7}Zr_{0.1}Y_{0.1}Yb_{0.1}O_{3-\delta}$ ($0.9 \leq x \leq 1.1$) proton conductors, Ceram. Int. 41 (2015) 7796–7802.

[25] K. H. Ryu, S. M. Haile, Chemical stability and proton conductivity of doped $BaCeO_3$ – $BaZrO_3$ solid solutions, Solid State Ionics 125 (1999) 355-367.

[26] K. Xie, R. Yan, Y. Jiang, X. Liu, G. Meng, A simple and easy one-step fabrication of thin BaZr0.1Ce0.7Y0.2O3-δ electrolyte membrane for solid oxide fuel cells, J. Membr. Sci., 325 (2008) 6-10.

[27] D. L. Corker, R. W. Whatmore, E. Ringgaars, W. W. Wolny, Liquid-phase sintering of PZT ceramics, J. Eur. Ceram. Soc. 20 (2000) 2039-2045.

[28] P. Babilo, T. Uda, S. H. Haile, Processing of yttrium-doped barium zirconate for high proton conductivity, J. Mater. Res., 22 (2007) 1322-1330.

[29] J. M. Serra, O. Büchler, W. A. Meulenberg, H P. Buchkremer, Thin $BaCe_{0.8}Gd_{0.2}O_{3-\delta}$ protonic electrolytes on porous $Ce_{0.8}Gd_{0.2}O_{1.9}$-Ni substrates, J. Electrochem. Soc., 154 (2007) B334-B340.

[30] D. K Lim, C. J. Park, M. B. Choi, C. N. Park, S. J. Song, Partial conductivities of mixed conducting $BaCe_{0.65}Zr_{0.2}Y_{0.15}O_{3-}\delta$, Int. J. Hydrogen Energy 35 (2010) 10624-10629.

[31] L. Malavasi, C. Tealdi, C. Ritter, V. Pomjakushin, F. Gozzo, Y. Diaz-Fernandez Combined neutron and synchrotron X-ray diffraction investigation of the $BaCe_{0.85-x}Zr_xY_{0.15}O_{3-\delta}$ ($0.1 \leq x \leq 0.4$) proton conductors, Chem. Mater. 25 (2011) 1323-1330.

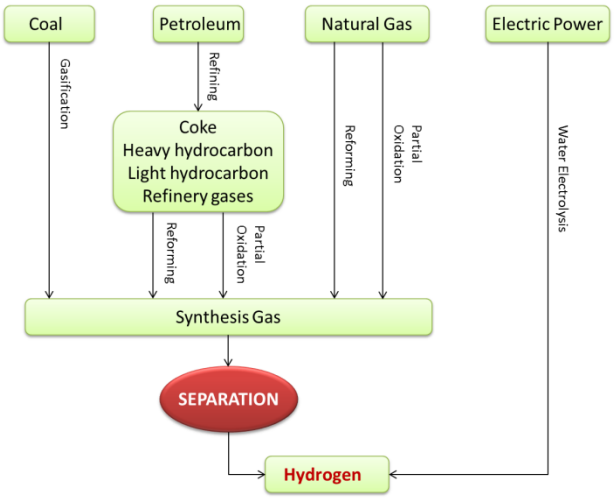

Figure 1 Schematic illustration of hydrogen production and separation [1].

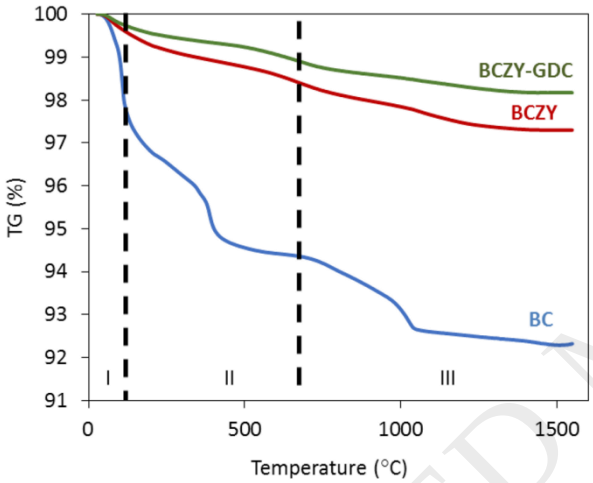

Figure 2 TGA of the BC, BCZY and BCZY-GDC powders used as Ba-sources.

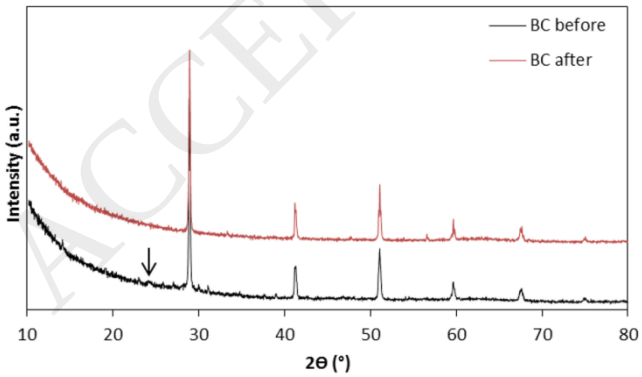

Figure 3 XRD analyses of the BC powder before and after the TGA. The arrow indicates the main peak of the $BaCO_3$ orthorhombic phase.

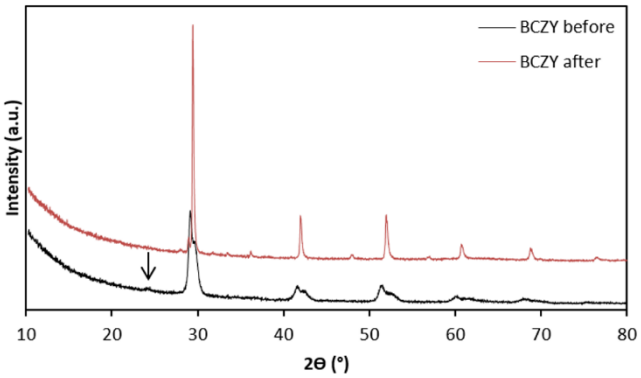

Figure 4 XRD analyses of the BCZY powder before and after the TGA. The arrow indicates the main peak of the $BaCO_3$ orthorhombic phase.

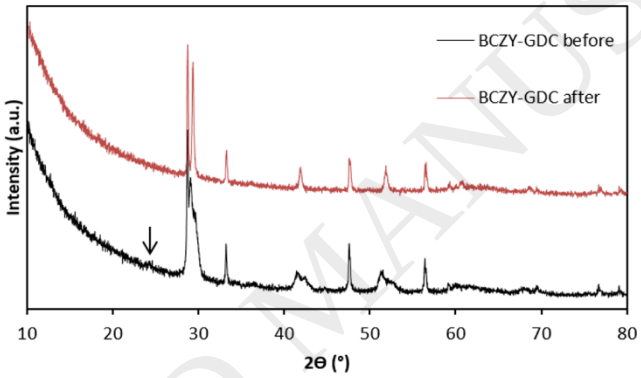

Figure 5 XRD analyses of the BCZY-GDC powder before and after the TGA. The arrow indicates the main peak of the $BaCO_3$ orthorhombic phase.

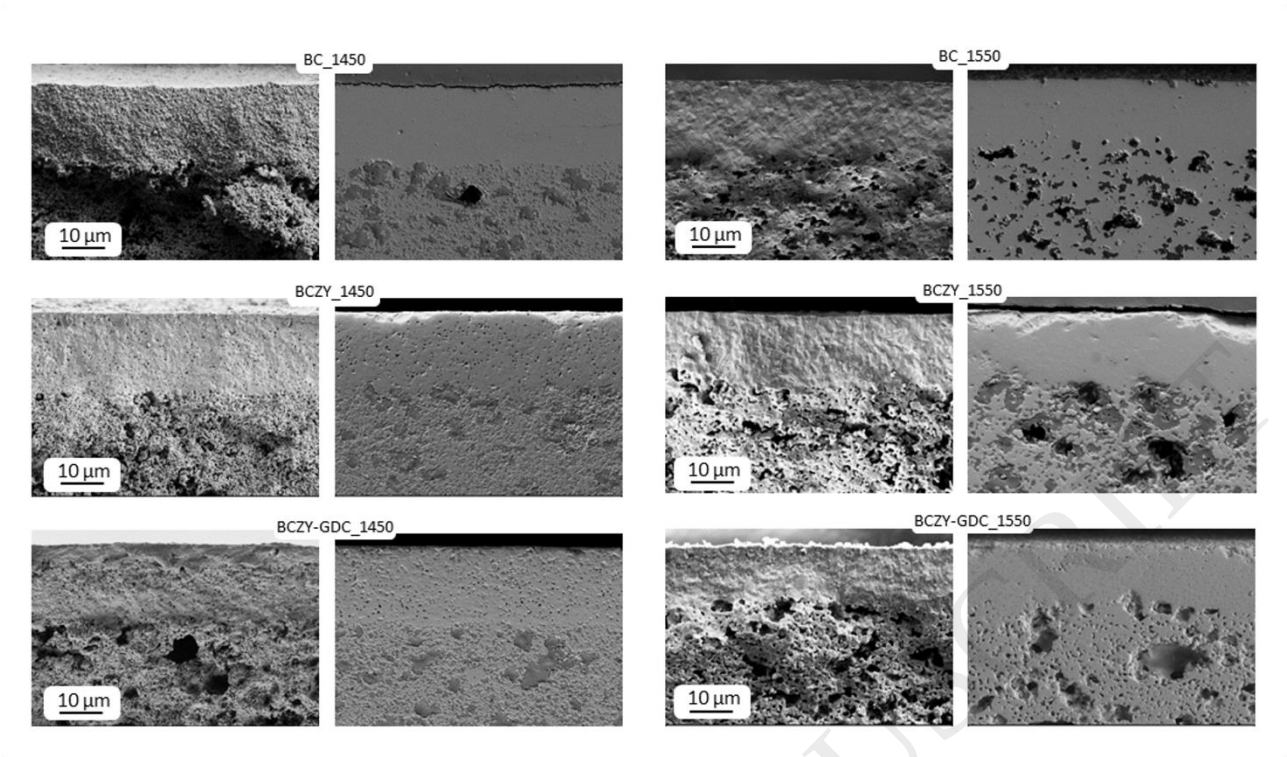

Figure 6 SEM micrographs of the fresh (on the left) and of the polished (on the right) cross sections of the asymmetric membranes sintered at 1450 and 1550°C using BC, BCZY and the mixture BCZY-GDC as Ba-sources.

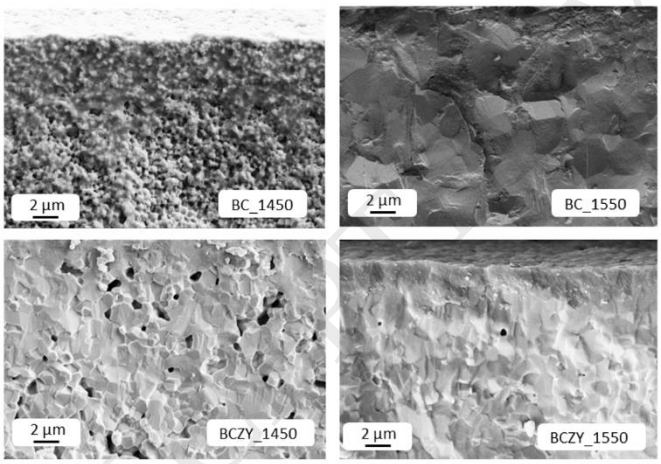

Figure 7 SEM micrographs at high magnification of the fresh cross section of the dense layer of the membrane sintered at 1450°C and 1550°C with BC and BCZY as Ba-sources.

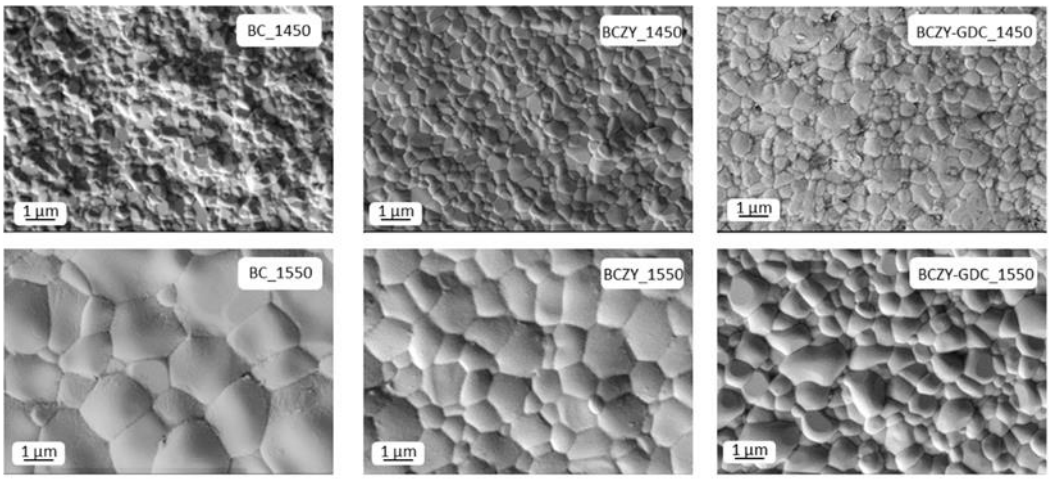

Figure 8 SEM analysis of the dense layer surfaces sintered at 1450 and 1550°C using: BC, BCZY and BCZY-GDC as Ba-sources.

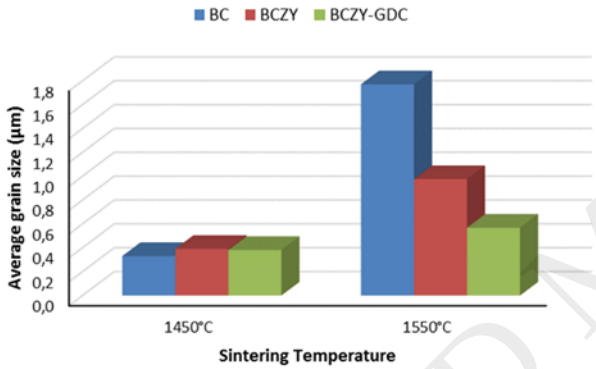

Figure 9 Average grain size of the membrane dense layers considered in this study.

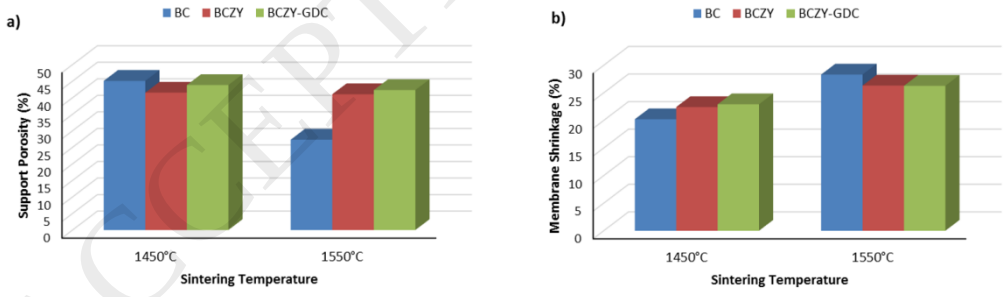

Figure 10 Porosity a) and values of shrinkage b) of the membrane support considered in this study.

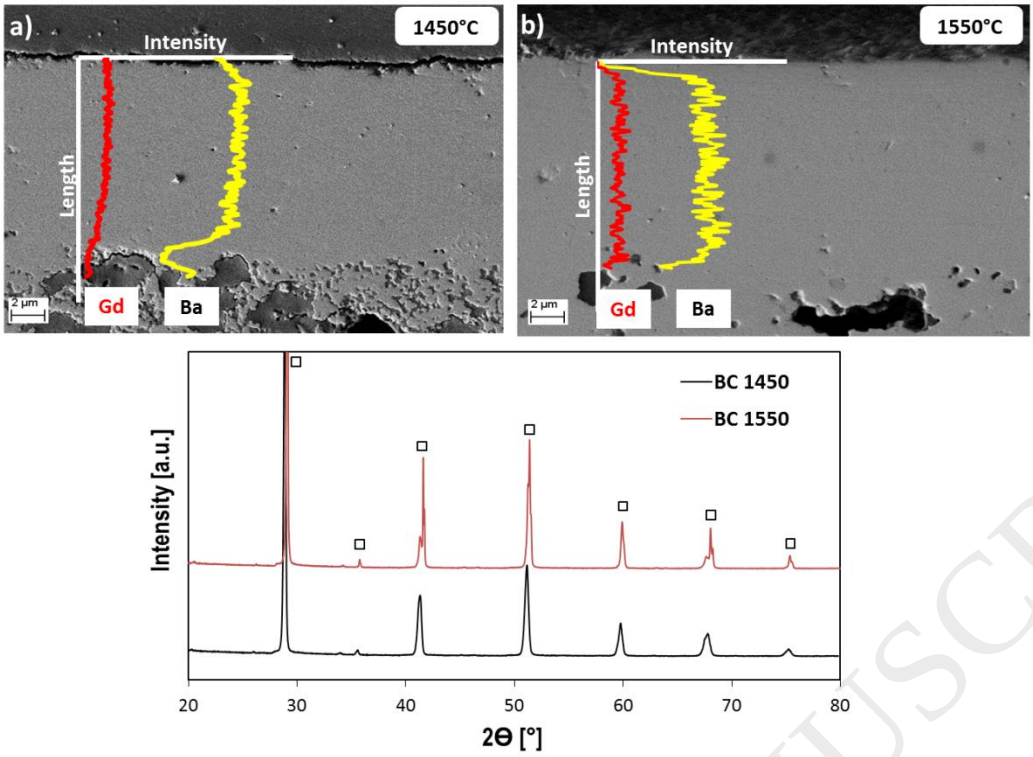

Figure 11 Back scattered SEM micrographs and Ba and Gd elements EDS profiles of the polished membrane section of the samples a) BC_1450 and b) BC_1550; c) XRD analyses of theBC_1450 and BC_1550 dense layer surface. The squares indicate the main peaks of the perovskite phase.

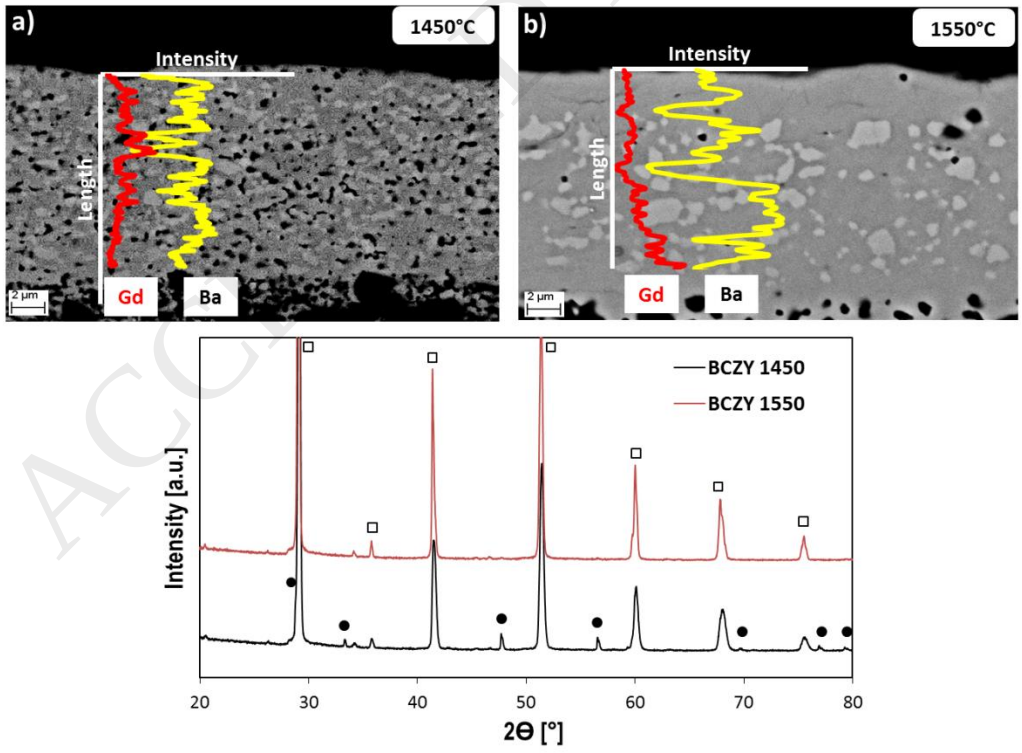

Figure 12 Back scattered SEM micrographs and Ba and Gd elements EDS profiles of the polished membrane section of samples a) BCZY_1450 and b) BCZY_1550; c) XRD analyses of the BCZY_1450 and 1550 dense layer surfaces. The squares and the dots indicate the main peak of the perovskite and GDC phase respectively

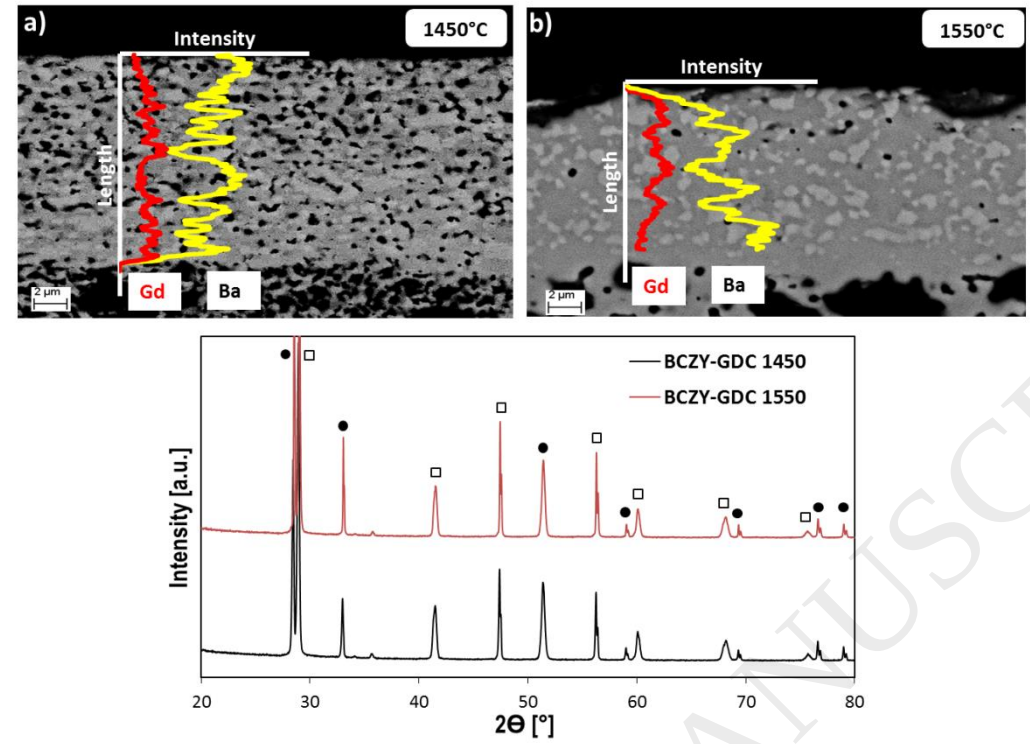

Figure 13 Back scattered SEM micrographs and Ba and Gd elements EDS profiles of the polished membrane section of samples a) BCZY-GDC_1450 and b) BCZY-GDC_1550; c) XRD analyses of the BCZY-GDC_1450 and 1550 dense layer surfaces. The squares and the dots indicate the main peak of the perovskite and GDC phase respectively.

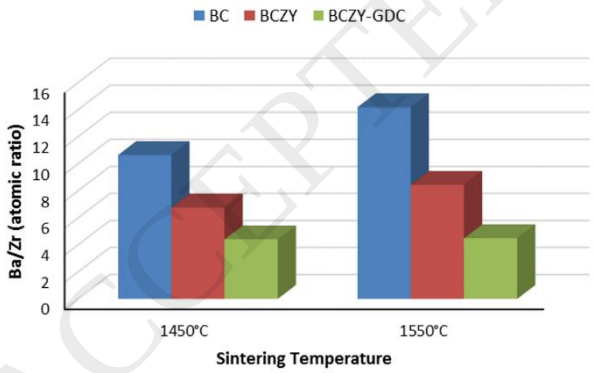

Figure 14 Ba/Zr atomic ratio values determined by EDS semi-quantitative analysis of the asymmetric membranes considered in this study.

Table 1 Ba/Ce atomic ratio values of the Ba-sources powders before and after being thermally treated at 1550°C for 4 hours determined by EDS semi-quantitative analysis.

	BC atomicBa/Ce	**BCZY atomic Ba/(Ce+Zr+Y)**	**BCZY-GDC atomic Ba/(Ce+Zr+Y+Gd)**
before	1.20 ± 0.02	1.11 ± 0.01	0.33 ± 0.01
after	1.04 ± 0.01	1.08 ± 0.02	0.33 ± 0.01

Table 2 Porosity of the membrane layers calculated by image analysis of the SEM polished section's micrographs.

	Residual porosity BC [vol.%]	**Residual porosity BCZY [vol.%]**	**Residual porosity BCZY-GDC [vol.%]**
1450°C	undetectable	4.7 ± 0.2	10.4 ± 0.2
1550°C	undetectable	0.7 ± 0.3	0.9 ± 0.4

Table 3 Phase composition, and lattice parameters of the main perovskite phase (prv) from XRD analyses on the dense surfaces of the sample considered in this study. Standard deviation is indicated within parentheses.

Sample name	**Phase/s**	**System**	**Space group**	**a [Å]**	**b [Å]**	**c [Å]**	**V [Å^3]**
BC_1450	BCZY-like	orthorhombic	*Pmcn*	8.7260(11)	6.1840(8)	6.2143(8)	335.33(13)
BC_1550	BCZY-like	orthorhombic	*Pmcn*	8.7238(19)	6.1960(13)	6.2122(13)	335.78(21)
BCZY_1450	BCZY-like	orthorhombic	*Pmcn*	8.7077(6)	6.1790(5)	6.1980(4)	333.48(6)
BCZY_1550	BCZY-like	orthorhombic	*Pmcn*	8.7183(6)	6.1841(4)	6.2057(5)	334.58(7)
BCZY-GDC_1450	BCZY	orthorhombic	*Pmcn*	8.6679(3)	6.1461(3)	6.1632(3)	328.34(2)
	GDC	cubic	*Fm*-3*m*	5.4107(1)	-	-	158.40(1)
BCZY-GDC_1550	BCZY	orthorhombic	*Pmcn*	8.6812(5)	6.1534(4)	6.1717(4)	329.69(4)
	GDC	cubic	*Fm*-3*m*	5.4151(2)	-	-	158.79(2)